PHOTONICS Research

Design of low-energy on-chip electro-optical 1 × *M* wavelength-selective switches

Richard Soref

Department of Engineering, The University of Massachusetts at Boston, 100 Morrissey Boulevard, Boston, Massachusetts 02125, USA (Richard. Soref@umb.edu)

Received 6 April 2017; revised 25 May 2017; accepted 2 June 2017; posted 7 June 2017 (Doc. ID 292262); published 10 July 2017

A theoretical design is presented for a 1 × *M* wavelength-selective switch (WSS) that routes any one of *N* incoming wavelength signals to any one of *M* output ports. This planar on-chip device comprises of a 1 × *N* demultiplexer, a group of *N* switching "trees" actuated by electro-optical or thermo-optical means, and an *M*-fold set of *N* × 1 multiplexers. Trees utilize 1 × 2 switches. The WSS insertion loss is proportional to $[\log_2 (M + N + 1)]$. Along with cross talk from trees, cross talk is present at each cross-illuminated waveguide intersection within the WSS, and there are at most *N* − 1 such crossings per path. These loss and cross talk properties will likely place a practical limit of $N = M = 16$ upon the WSS size. By constraining the 1 × 2 switching energy to ∼1 fJ/bit, we find that resonant, narrowband 1 × 2 switches are required. The 1 × 2 devices proposed here are nanobeam Mach–Zehnders and asymmetric contra-directional couplers with grating assistance.

OCIS codes: (060.4230) Multiplexing; (130.4815) Optical switching devices; (130.6622) Subsystem integration and techniques.

https://doi.org/10.1364/PRJ.5.000340

1. INTRODUCTION

The wavelength-selective switch (WSS) is an essential component in reconfigurable wavelength-division multiplexed (WDM) systems, especially in data center and high-performance computing applications. The recent article by Sahara *et al.* [1] shows how a group of 1 × *KM* WSSs could enable a capable space-division node in which several multi-core optical fibers exchange WDM signals in a reconfigurable manner. The approach taken to realize WSSs in recent commercial products is predominantly a "free-space optics" approach—a full 3D realization using liquid crystals or microelectromechanical systems or spatial light modulators. A 2D approach is less studied. A WSS challenge that has not been met is to realize a large-scale WSS in planar 2D form by means of an integrated-photonics network on a silicon chip. That 2D WSS is the focus of this paper.

The 2D approach offers semiconductor chip manufacture, unlike the 3D approach. The 3D free-space approach uses massively parallel optical paths and the scatter-free intersection of light beams, but the 2D method takes those same 3D optical paths and "condenses" them into one plane, a compression that requires waveguide intersections. Thus the 2D method has the disadvantage of introducing some cross talk (CT) at each waveguide crossing in the planar network.

2. PROPOSED WSS APPROACH

By definition, the WSS routes each one of the *N* independent wavelength-channel signals traveling within a common shared waveguide to any one of *M* output ports. To attain the 2D WSS, we build upon a concept reported in the literature—first, to demultiplex or "disperse" the *N* signals, then to send them into an *N*-fold array of wavelength-specific 1 × *M* switches, and finally to multiplex the resulting *MN* outputs onto *M* waveguided output paths. An innovation here is the use of a 1 × *M* equal-branch "tree" architecture in which the insertion loss (IL) of the device is the same, irrespective of the optical path selected within the switch. The main novelty here is the resonance discussed in Section 3 below.

The approach here features thermo-optic (TO) or electro-optic (EO) actuation of the 1 × 2 tree-constituent switches, which are actually 2 × 2 switches with the add port dangling. The WSS goals are high figures of merit along with cost-effective manufacturing of the chips in a foundry. Silicon photonics, such as the silicon-on-insulator (SOI) CMOS platform, is ideal for WSS manufacturing, because the silicon photonics industry is gearing up for large-scale integration. All of the active devices proposed here have nanometer-scale features that a modern factory node is capable of realizing.

The WSS is part of a WDM on-chip system. The following goals were used in designing this switch: (1) the WSS IL and optical CT should be low enough for "large" *N* and *M*, (2) an individual wavelength or a set of wavelengths is routed to any one of *M* output ports, and (3) the energy required for the digital switching of each 1 × 2 component within the WSS should be ∼1 fJ/bit. An immediate consequence of the 1 fJ/bit constraint is that *resonant*

or narrowband 1 × 2 constituents must be chosen to realize the WSS.

Narrowband implies a very small mode volume within the active zone of each waveguided 1 × 2. Narrowband provides low energy, since the dynamic switching energy is proportional to the mode volume. (There may or may not be a DC holding energy for state 1 of the 1 × 2*s*). Resonance is helpful, since a small change in the effective index of the mode volume (Δn) will be sufficient to change the state of the switch from state 1 to state 2. EO actuation gives the ~1 fJ/bit feature, while the TO switch control offers proof of principle in initial experiments as well as submilliwatt switching power. We present in this paper three 2 × 2 devices—detailed below—that have the ultrasmall active volume.

3. PRIOR-ART 2D INTEGRATED WSS

During the past five years, several practical 2D integrated on-chip WSSs have been developed and tested experimentally [2–7]. These designs and experimental devices utilize broadband 1 × 2 (or 2 × 2) TO switches based on the Mach–Zehnder interferometer (MZI) architecture. In several of the WSSs [2–5] the functions of demultiplexing (demux) and multiplexing (mux) are performed by passive arrayed-waveguide gratings (AWGs), while in Ref. [6] those functions are done by a group of microring resonator devices, each consisting of two bus waveguides coupled to the ring. In Ref. [7] planar concave gratings serve for mux/demux. By contrast to the prior art, the WSS novelty here is in the use of resonant EO 1 × 2 switches together with those same resonant structures being employed in a passive or unswitched mode in order to carry out the mux and demux tasks (see Section 9 below).

4. PROPOSED WSS ARCHITECTURE

Figure 1 shows how the inplane color routing would be achieved. The lines represent channel waveguides connecting the components. Each tree has an equal-branching arrangement and is resonant at one of the input wavelengths. The initial splitting (demux) and the later recombining (mux) of wavelength signals is shown. For the passive demux/mux devices sketched here, there are several good possibilities. One of these is the AWG, well known in the silicon photonics art.

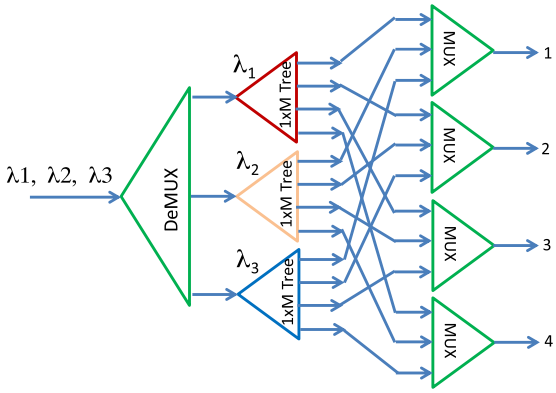

Fig. 1. Schematic diagram of proposed WSS employing an *N*-fold set of wavelength-dedicated 1 × *M* equi-path switching trees.

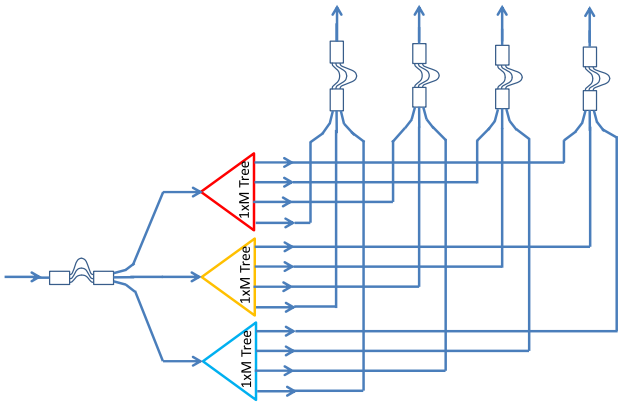

Fig. 2. Implementation of Fig. 1 utilizing inplane 1 × 3 and 3 × 1 arrayed-waveguide grating devices for the demux and mux sections.

We have presented the AWG WSS in Fig. 2, where we have substituted a simple regular pattern of orthogonal intersections for the complex intersections in Fig. 1.

5. PROPOSED 1 × 2 AND 1 × *M* RESONANT SWITCHES

It is suggested here that the switching trees are implemented by cascading 1 × 2 switches, each of which is a resonant 2 × 2 "cross bar" device with one of its input ports dangling. Specifically, three versions of the "practical tree" for the silicon photonics art are illustrated. Each tree uses different 1 × 2*s* as follows. Figure 3 shows the dual-nanobeam MZI detailed in Ref. [8], while Fig. 4 presents an MZI in which each 3 dB coupler has been replaced by a three-waveguide coupler (3W) in which the central island is an active nanobeam. This Fig. 4 switch has been realized recently [9]. Finally, the tree in Fig. 5 shows an asymmetric contra-directional coupler in which the active coupling zone comprises two Bragg gratings that have been offset by a π rad phase shift segment. This proposed switch has been discussed in Ref. [10].

The Fig. 3 switches use optical engineering of the air hole lattice to attain high transmission of the fundamental mode of this 1D photonic crystal waveguide [8], thereby giving—for state 1—a strong peak of transmission at the through port and a notch at the drop port. Looking at each 3W in Fig. 4,

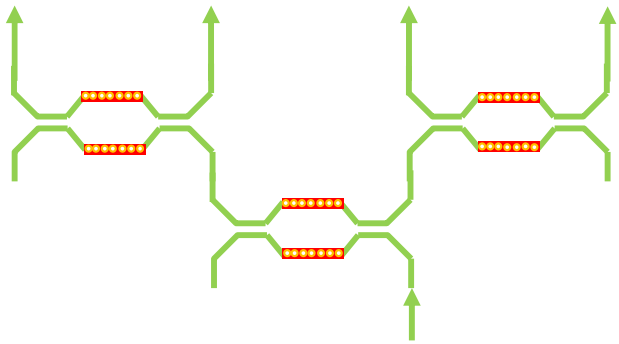

Fig. 3. Waveguide diagram of 1 × 4 tree utilizing dual-nanobeam MZIs as the 1 × 2 constituent switches.

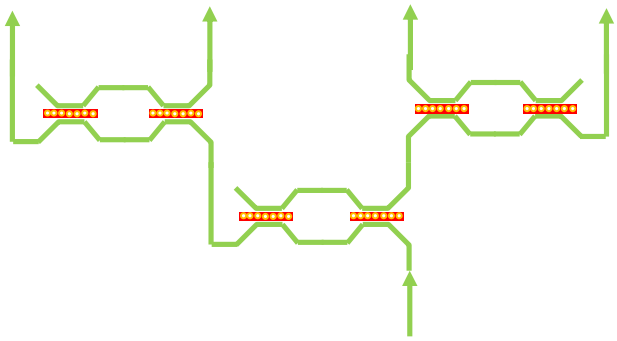

Fig. 4. Waveguide diagram of 1 × 4 tree utilizing MZI constituent 1 × 2 switches composed of a pair of three-waveguide couplers, each containing a central nanobeam.

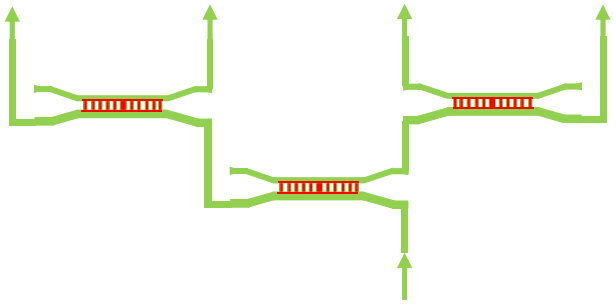

Fig. 5. Waveguide diagram of 1 × 4 tree using asymmetric contra-couplers as 1 × 2 elemental switches, each switch containing an offset dual-grating coupling region.

25% of the input exits at each of four ports. To get constructive interference of those reflection components, it is necessary to introduce optical phase delays in the two connecting waveguide arms of the MZI as prescribed in Ref. [11], phase shifts that give, according to coupled mode theory, "total" transmission of the input light to the through port in state 1. Those phase delays are attained by making one arm slightly longer than the other [9].

The Fig. 5 switches employ waveguides of slightly different widths to suppress codirectional forward coupling. The device is resonant at the phase-matching wavelength between the two super modes. Reflection back to the input is avoided, and the resonant reflection goes to the drop port [10].

Regarding the active region(s) in Figs. 3, 4, and 5, we have not shown the control electrodes in order to keep those diagrams simple. In Figs. 3 and 4, there would be a lateral PN or PIN diode in the central part of each nanobeam (a few micrometers long) to shift the Bloch-1 mode spectrum along the wavelength axis via the free carrier plasma effect, or there would be an electrical strip resistance heater on each nanobeam center for TO shifting. A unique and important feature in Fig. 5 is that an individual waveguide is not selectively perturbed by EO or TO. Instead, the centralized inter-guide grating is perturbed symmetrically by EO or TO means, giving an equal change in index on each side of the longitudinal axis. For TO, one heater along the grating axis will suffice. For completeness, we should add that there are two more 1 × 2 narrowband EO or TO devices (not shown here) that could serve well in the 1 × 4 tree task. These are the microring-assisted MZI [12] and the slow-light MZI [10].

6. TYPICAL CHARACTERISTICS OF 1 × 2*s*

Let's consider the SOI platform with wavelengths in the 1530 to 1570 nm range, and let's examine the performance that can be achieved in practice for the elemental 1 × 2 switches in Figs. 3, 4, and 5. Modeling and simulation of the 1 × 2*s* in Fig. 3 were performed in Ref. [8]. Theoretical estimates of the optical IL optical CT and energy per bit E were given and are cited here. These are for C-band silicon rib-waveguide nanobeams with a 50 nm rib platform and with local P and N doping to form a lateral PN junction at the nanobeam cavity midline, where the active length for EO modulation (the doping length) was 2 μm. The cross state occurred at +0.53 V applied, while the bar state was reached at −2.16 V applied. The waveguide core dimensions were $W \times H$ of 500 nm × 220 nm. Along the nanobeam axis, a 1D photonic crystal lattice of 24 air holes had their diameter tapered in and out quadratically to form a zero point-defect cavity for TE-polarized light.

From that geometry, IL(cross) = 2.0 dB and CT(cross) = −16 dB were estimated together with IL(bar) = 0.5 dB and CT(bar) = −16 dB. Additional unpublished simulations show an IL(cross) of 1.5 dB after optimization of the nanobeam geometry. The WSS described in Section 9 below includes a set of unswitched Fig. 3 dual nanobeam MZI devices that serve as add–drop multiplexers. These passive 1 × 2 devices do not have any electrodes. They are not doped and are made of intrinsic silicon. As a result, the throughput loss is lower. Unpublished simulations of those passives indicate that IL(cross) = IL(bar) = 1 dB.

Turning to the 1 × 2*s* in Fig. 4, the modeling and simulations in Ref. [13] for PN depletion of dual 3W nanobeams indicate IL(cross) = 1.2 dB and CT(cross) = −14.2 dB at +0.89 V, as well as IL(bar) = 0.4 dB and CT(bar) = −13.4 dB obtained at −2.79 V. Returning to the 1 × 2*s* in Fig. 3, it should be noted that the IL is reduced when PIN injection is employed as an alternative to PN depletion. For example, the largest IL (bar state) becomes 0.97 dB according to theory simulations for a 2 × 2 Ge PIN nanobeam MZI at 2.1 μm [14]. However, then the required 1 × 2 switching energy is much higher.

Why is IL different in the cross and bar states of the 1 × 2 switches? For the bar state, high transmission is obtained from the off-resonance characteristic of the wavelength-shifted spectrum. For the cross state, both the lattice design and the absorption component of the free carrier plasma (the P and N doping) govern IL. Both of these determine the Q and the on-resonance transmission percentage.

The 1 × 2 switching energy per bit is the sum of the energy consumed in state 1 and the energy consumed in state 2, specifically, $E = \frac{1}{2}(C_f V_1^2 + C_r V_2^2)$, where C_f is the nanobeam junction capacitance in the forward-biased state at voltage V_1 and C_r is the capacitance in the reverse-biased state at V_2. Here the most critical factor is the bias-dependent C_f. This E includes both nanobeams and assumes a digital logic

format. Lumerical device simulations in Ref. [8] reveal that $C_f = 0.55$ fF at +0.53 V, whereas $C_r = 0.17$ fF at –2.16 V. Using the above formula, we estimate that $E = 0.5$ fJ/bit. Regarding the three metrics of IL, CT, and E, the values of those parameters for the $1 \times 2s$ in Fig. 5 have not yet been investigated but are anticipated to be rather close to those cited here for the $1 \times 2s$ in Fig. 3.

7. ANALYSIS OF $1 \times M$ TREES

Looking at the tree elements in Figs. 3, 4, and 5, each 1×2 has a Q defined as $\lambda/\Delta\lambda$, where λ is the operation wavelength within in the resonance spectral "profile" and $\Delta\lambda$ is the spectral passband of that channel. In a WDM system, the information bandwidth per channel is typically 50 to 100 GHz; therefore, at $\lambda = 1550$ nm, we are seeking $\Delta\lambda$ within the 0.4 to 0.8 nm range, prescribing a Q that goes from 3875 down to 1938. For the elemental $1 \times 2s$ discussed here, the principle of operation of the switch is to shift the "resonance profile" along the wavelength axis by an amount $\Delta\lambda_s$, a translation caused by TO- or EO-induced Δn. Considering the bandwidth $\Delta\lambda$, the desire for a large information bandwidth comes into conflict with a desire to make $\Delta\lambda$ small so that $\Delta\lambda_s$ can easily exceed $\Delta\lambda$. This $\Delta\lambda_s > \Delta\lambda$ relation is advantageous to provide low CT in the 1×2. The relative sizes of $\Delta\lambda$ and $\Delta\lambda_s$ that are needed depend on the device specifics and actuation method. Generally $\Delta\lambda_s = r\Delta\lambda$ is required, where r is 0.6 to 2.0. In practice, there is an upper limit of $r \sim 2$ imposed by TO and EO physics.

Although a high Q around 10,000 is feasible in the proposed $1 \times 2s$, these Q values are ruled out for two reasons: (1) the channel bandwidth would be too small, and (2) the requirements on thermal stability and resonance targeting would be too stringent. Even at our 1×2 goal of $Q \sim 3000$, a price must be paid for the low-energy switching. The resonant system-on-a-chip demands compromise and trade-offs. There are problems in aligning the input wavelengths with the resonances and in maintaining these alignments in the environment. In addition, fabrication must be accurate. High precision must be attained in the construction of the nanobeam and grating-coupled devices in Figs. 3, 4, and 5 to assure that every 1×2 within the $1 \times M$ tree has the same spectral line shape. If the spectral profiles within a tree are not identical, then the spectral bandpass of the tree will be compromised and reduced. To achieve the desired tree fabrication, it will probably be necessary to implement switches in an advanced 45 nm SOI CMOS foundry node, as was discussed in Ref. [11]. Summarizing our resonant approach to low-energy trees, we see that achieving the major reduction in energy brings with it a new set of challenges.

8. WAVELENGTH-DIVISION MULTIPLEXING

The WDM operation of Fig. 1 can be understood by examining the response of any 1×2 within a given tree. These $1 \times 2s$ have a drop port and a through port as their two outputs. Now let us hypothesize a multichannel WDM application that uses a 2 nm λ-channel spacing and a resonance width of ~0.4 nm for the switches. We can see how the trees of Figs. 3, 4, and 5 function by looking at the schematic in Fig. 6.

This optical transmission diagram illustrates the two-output-port switching of a particular wavelength (λ_3 for

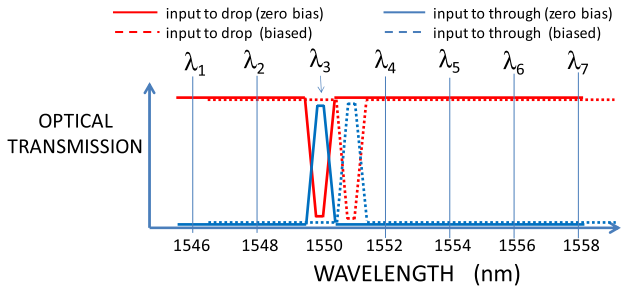

Fig. 6. Overall spectral response of the switches in Figs. 3, 4, and 5 in the zero bias state (unshifted spectrum) and in the full-bias state (shifted spectrum).

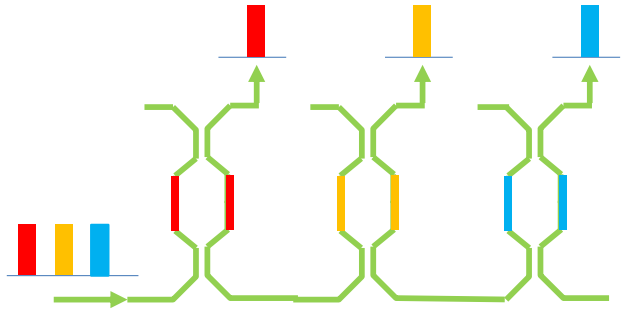

Fig. 7. Passive demultiplexing of a multiwavelength input stream using a sequence of dedicated-resonance 2×2 devices (the example of the Fig. 3 structure).

example) within the 1D photonic crystal forbidden gap as well as the "passing through" of all the other wavelengths well outside of the resonance [8]. Related to this switching-and-passing behavior is the passive demux or mux response of an undisturbed (unbiased) 1×2. Taking the example of the dual nanobeam MZI, we have illustrated in Fig. 7 the convenient and effective demux that is available for the example of $N = 3$. Because of the beneficial drop/pass Fig. 7 features, we shall apply the Fig. 7 demux/mux approach to the overall WSS.

9. PROPOSED WSS ARCHITECTURE

Because the "replication" of integrated photonic components is well suited to manufacturing, it is beneficial to use the same structure (such as the MZI layout) for every component within the WSS. In this spirit, Fig. 8 shows a WSS with $N = 3$ and $M = 4$ in which the dual nanobeam device is used everywhere, either passively for demux/mux or actively for trees. The color coding of red, orange, and blue shows how each 1×2 resonance is mapped to a particular incident wavelength.

10. ANALYSIS OF WSS

Regarding the trees in Fig. 8, there is a fundamental physics problem about the information bandwidth of each tree, a bandwidth defined by the "product" of 1×2 switches connected in a series or cascade (the multiplied profile). For example, if we assume that each 1×2 is identical (that the technology problem is solved), and if we take the spectral linewidth of each 1×2 to be

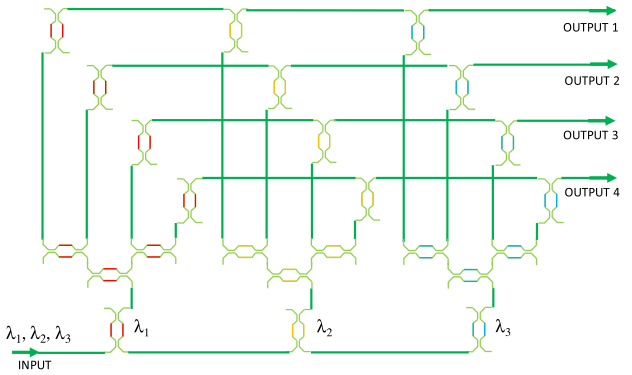

Fig. 8. Proposed design of three-wavelength, four-output WSS utilizing Fig. 3 devices.

400 pm, as in Fig. 6, then we can apply a mathematical analysis to find out how much the 1 × 2 bandwidth is shrunk within a tree. To be specific, let us assume a Gaussian profile for the 1 × 2 switches and calculate the linewidth of the tree as a function of the number of stages q per tree. The results are $\Delta\lambda = 267$ pm for $q = 2$, 222 pm for $q = 3$, 200 pm for $q = 4$, and 186 pm for $q = 5$. Some applications are impacted negatively by this narrowing. Regarding a possible reduction of WSS bandwidth resulting from the cascaded demux and mux devices in Fig. 8, we can alleviate that bandpass shrinkage by widening the demux/mux linewidth from 0.4 nm in Fig. 6 to 1.0 or 1.2 nm in Fig. 8, a widening that does not injure the mux. Similarly, by employing the AWG mux technique in Fig. 2 (instead of the 1 × 2 muxes of Fig. 8), bandwidth narrowing within the WSS can be avoided for ~1-nm-wide mux channels.

The WSS IL and CT on any input-to-output path are now estimated. Examination of Fig. 8 shows that IL and CT are path dependent. Referring to Fig. 8, we see that each tree has q stages where $2^q = M$ and $q = \log_2 M$. Looking first at the active $1 \times 2s$, we note that the state-1 IL usually differs from the state-2 IL. Let us assume that the 1 × 2 IL L is the larger of those two IL values. Thus a tree contributes a loss of qL. However, there is fixed loss $\mathcal{L}$ in the Fig. 8 demux, plus a *variable* loss in the mux. Adding up the active and passive 1 × 2 losses along a given path, we find that the overall IL in Fig. 8 ranges from $qL + 2\mathcal{L}$ up to $qL + (N + 1)\mathcal{L}$, the latter being the limiting value—not counting any propagation loss in the connecting network.

Returning for a moment to Fig. 2, where AWG muxes are deployed, it is found that the overall IL is the same for any selected path within the WSS. Under the optimistic assumption that each AWG produces an IL that is the same as $\mathcal{L}$ cited above, then the WSS IL in Fig. 2 is $qL + 2\mathcal{L}$. Therefore, the Fig. 2 WSS is superior to the Fig. 8 WSS in the aspect of IL being path independent.

Turning to the CT in Fig. 8, there are two contributions to overall WSS CT: the CT from trees and the CT from waveguide intersections. Considering the trees, if each 1 × 2 has a particular CT level, that amount of "noise" will appear at some tree outputs, after which that CT is muxed to the WSS outputs. For an individual 1 × 2 in the tree, *cts* represents the largest CT value of the switch (state 1 or state 2). That *cts* becomes attenuated as it travels through the mux portion of the WSS. This *cts* damping is $(q - 1)L$ within the tree, plus $\mathcal{L}$ for the mux (worst case). Therefore the tree-originated WSS CT = *cts*(dB) – $(q - 1)L$(dB) – $\mathcal{L}$(dB) in the worst case scenario. For example, referring to the above-cited *cts* = –16 dB as well as the $L = 1.5$ dB and $\mathcal{L} = 1.0$ dB estimates in Section 6 above, the Fig. 8 CT($q = 2$) is –18.5 dB or less.

Next we analyze the CT arising from several waveguide crossings. The number of crossings that is attached to a given WSS output is variable. Examining Fig. 8, there are zero to $(N - 1)(M - 1)$ crossings per output. However, some crossings do not contribute to CT. Along a WSS input-to-output path, there are illuminated and dark intersections. "Illuminated" means that a unitary light beam crosses the main waveguide, while "dark" means that the cross beam is not present or is very weak. A path-tracing analysis is used to find the total number of light and dark crossings. We neglect all dark crossings and assume no CT contribution from them. Taking the representative case of $M = N$, we find that at most $N - 1$ "illuminateds" are on a path. This is the limiting case of CT for the WSS. If we define *ctx* as the CT of one unit-illuminated crossing, then CT = $(N - 1)$*ctx*. The literature about waveguide intersection design indicates that SOI channel crossings can be engineered to have a *ctx* as low as –30 dB, which is an 0.001 noise power transmission. Assuming that transmission, then the above crossing analysis gives an $(N - 1)(0.001)$CT transmission.

Now let's examine two WSS cases, $M = N = 8$ ($q = 3$) and $M = N = 16$ ($q = 4$), in an effort to determine the practical upper limit on WSS size. Looking first at loss in Fig. 8, the overall IL has a maximum of $3L + 9\mathcal{L}$ for $M = 8$, and of $4L + 17\mathcal{L}$ for $M = 16$, whereas in Fig. 2 the losses are $3L + 2\mathcal{L}$ at $M = 8$ and $4L + 2\mathcal{L}$ at $M = 16$. Taking $L = 1.5$ dB and $\mathcal{L} = 1.0$ dB as described above, then the largest loss in Fig. 8 is 13.5 dB for $M = 8$ and 23 dB for $M = 16$, which might restrict Fig. 8 to $M = 8$. However, the Fig. 2 approach would have only 8 dB of loss at $M = 16$, suggesting practicality for that WSS. Considering the overall CT in Fig. 8, the worst-case tree contribution is –[16 + 2(1.5) + 1] dB = –20 dB for $M = 8$, and –[16 + 3(1.5) + 1] dB = –21.5 dB for $M = 16$, whereas the worst-case $(N - 1)(0.001)$ crossing CT in Fig. 8 is l0lg0.007 for $M = 8$ and 10lg0.015 for $M = 16$, which is –21.5 dB and –18.2 dB, respectively. Adding both contributions, the overall CT result is –20.1 dB at $M = 8$ and –18.2 dB at $M = 16$. The foregoing analysis shows that both IL and CT come into play to place an upper limit on M, and it can be argued from the specifics that $M = 16$ is marginally acceptable, while $M = 8$ is practical.

Regarding the WSS total energy consumption, if E is the 1 × 2 switching energy, then the addressing energy of the WSS is NqE because q devices are active in each of N trees. This gives $24E$ for $N = M = 8$ and $64E$ for $N = M = 16$, which is still in the low fJ/bit range for the above 0.5 fJ/bit example of E. For the $M > N$ cases, the number of stages q can be higher than for $M = N$ cases, but the total energy still scales as N.

11. CONCLUSION

An inplane N-wavelength WSS with M outputs and demux–tree–mux architecture has been proposed for applications in CMOS-compatible WDM chip systems. To satisfy the requirement of

ultralow dynamic switching energy, resonant 1 × 2 EO switching devices have been proposed for the equi-branched $1 \times M$ trees and for the passive add–drop mux. The 1 × 2 devices proposed are nanobeam MZIs and grating-assisted contradirectional couplers. Analysis of the WSS's overall IL, CT, and E has been performed, and the combination of these metric results suggests a practical upper limit of $N = M = 16$ on the WSS size.

Funding. Air Force Office of Scientific Research (AFOSR) (FA9550-14-1-0196).

REFERENCES

1. A. Sahara, H. Kawahara, S. Yamamoto, S. Kawai, M. Fukutoku, T. Mizuno, Y. Miyamoto, K. Suzuki, and K. Yamaguchi, "Proposal and experimental demonstration of SDM node enabling path assignment to arbitrary wavelengths, cores, and directions," Opt. Express **25**, 4061–4075 (2017).
2. H. Asakura, K. Sugiyama, and H. Tsuda, "Design of a 1 × 2 wavelength selective switch using an arrayed-waveguide grating with fold-back paths on a silicon platform," in *Optoelectronics and Communications Conference* (2016), paper WA2-105.
3. H. Asakura, T. Yoshida, H. Tsuda, K. Suzuki, K. Tanizawa, M. Toyama, M. Ohtsuka, N. Yokoyama, K. Matsumaro, M. Seki, K. Koshino, K. Ikeda, S. Namiki, and H. Kawashima, "A 200-GHz spacing, 17-channel, 1 × 2 wavelength selective switch using a silicon arrayed-waveguide grating with loopback," in *2015 International Conference on Photonics in Switching* (2015).
4. Y. Ikuma, T. Mizuno, H. Takahashi, T. Ikeda, and H. Tsuda, "Low-loss integrated 1 × 2 gridless wavelength selective switch with a small number of waveguide crossings," in *European Conference and Exhibition on Optical Communication* (2012), paper Tu.3.E.5.
5. C. R. Doerr, L. L. Buhl, L. Chen, and N. Dupuis, "Monolithic flexible-grid 1 × 2 wavelength-selective switch in silicon photonics," J. Lightwave Technol. **30**, 473–478 (2012).
6. K. Miura, Y. Shoji, and T. Mizumoto, "Silicon waveguide wavelength-selective switch for on-chip WDM communications," in *IEEE Photonics Conference (IPC)* (2012), pp. 630–631.
7. J. Song, X. Luo, Q. Fang, L. Jia, X. Tu, T. Liow, M. Yu, and G. Lo, "Silicon-based 2 × 2 colorless wavelength selective switch for optical interconnect application," in *Optical Fiber Communication Conference*, OSA Technical Digest (2012), paper OM2J.2.
8. R. Soref and J. Hendrickson, "Proposed ultralow-energy dual nanobeam devices for on-chip N × N switching, logic and wavelength multiplexing," Opt. Express **23**, 32582–32596 (2015).
9. H. Zhou, C. Qiu, X. Jiang, Q. Zhu, Y. He, Y. Zhang, Y. Su, and R. Soref, "Compact, submilliwatt, 2 × 2 silicon thermo-optic switch based on photonic crystal nanobeam cavities," Photon. Res. **5**, 108–112 (2017).
10. R. Soref, "Resonant and slow-light 2 × 2 switches enabled by nanobeam and grating-coupled waveguides," in *Session IP5 at Progress in Electromagnetics Research Symposium (PIERS) (Invited Paper)* (2017).
11. C. V. Poulton, X. Zeng, M. T. Wade, and M. A. Popovic, "Channel add-drop filter based on dual photonic crystal cavities in push-pull mode," Opt. Lett. **40**, 4206–4210 (2015).
12. L. Lu, L. Zhou, Z. Li, X. Li, and J. G. Chen, "Broadband 4 × 4 nonblocking silicon electrooptic switches based on Mach-Zehnder interferometers," IEEE Photon. J. **7**, 7800108 (2015).
13. H. Zhou, C. Qiu, J. Wu, B. Liu, X. Jiang, J. Peng, Z. Xu, Y. Zhang, R. Liu, Y. Su, and R. Soref, "2 × 2 electro-optical switch with fJ/bit switching power based on dual photonic crystal nanobeam cavities," in *Conference on Lasers and Electro-Optics*, OSA Technical Digest (2016), paper JTh2A.
14. R. Soref, J. R. Hendrickson, and J. Sweet, "Simulation of germanium nanobeam electro-optical 2 × 2 switches and 1 × 1 modulators for the 2 to 5 μm infrared region," Opt. Express **24**, 9369–9382 (2016).